nature biotechnology

ARTICLES

https://doi.org/10.1038/s41587-019-0090-6

Highly efficient expression of circular RNA aptamers in cells using autocatalytic transcripts

Jacob L. Litke[1,2] and Samie R. Jaffrey[1,2*]

RNA aptamers and RNA aptamer-based devices can be genetically encoded and expressed in cells to probe and manipulate cellular function. However, their usefulness in the mammalian cell is limited by low expression and rapid degradation. Here we describe the Tornado (Twister-optimized RNA for durable overexpression) expression system for achieving rapid RNA circularization, resulting in RNA aptamers with high stability and expression levels. Tornado-expressed transcripts contain an RNA of interest flanked by Twister ribozymes. The ribozymes rapidly undergo autocatalytic cleavage, leaving termini that are ligated by the ubiquitous endogenous RNA ligase RtcB. Using this approach, protein-binding aptamers that otherwise have minimal effects in cells become potent inhibitors of cellular signaling. Additionally, an RNA-based fluorescent metabolite biosensor for *S*-adenosyl methionine (SAM) that is expressed at low levels when expressed as a linear RNA achieves levels sufficient for detection of intracellular SAM dynamics when expressed as a circular RNA. The Tornado expression system thus markedly enhances the utility of RNA-based approaches in the mammalian cell.

RNA aptamers are short RNAs that bind intracellular molecules or proteins and can thus modulate intracellular processes[1,2]. Because aptamers can bind specific domains[3] and conformations[4] of proteins, they can either inhibit proteins or modulate their function. Despite their potential applications, RNA aptamers have not achieved anywhere near the level of widespread use as other RNA-based technologies such as small interfering RNAs or guide RNAs.

The major problem with RNA aptamers is that they cannot be expressed at sufficiently high concentrations to efficiently modulate protein function. When expressed using the U6 promoter, the most effective promoter for small RNA expression[5], RNA aptamers achieve concentrations in the low nanomolar range and exhibit half-lives ranging from 0.25 to 1.25 h[6]. However, proteins are often expressed in the high nanomolar or even micromolar range in cells[7], meaning that aptamer concentrations are too low for stoichiometric regulation of target proteins.

Low expression levels also prevent the use of RNA devices, such as genetically encoded RNA-based metabolite biosensors, in mammalian cells. These biosensors are RNA transcripts that comprise a fluorogenic RNA aptamer such as Spinach[8] and an aptamer that binds a metabolite[9–11]. Routine design of these biosensors[12] has enabled fluorescence imaging of diverse metabolites and signaling molecules in bacteria[9–11]. However, unlike in bacteria, where these RNA-based metabolite biosensors accumulate to micromolar concentrations[9], these RNA devices are expressed at nanomolar concentrations in mammalian cells[6]. As a result, these biosensors produce undetectable fluorescence signals in mammalian cells.

Here we describe a novel expression system that achieves high-level expression and functional activity of RNA aptamers and RNA devices in mammalian cells. With this approach, RNAs are stable because they are rapidly and efficiently circularized. Circularization is achieved without the co-expression of any additional proteins or enzymes. To trigger RNA circularization, RNA transcripts are expressed containing an RNA of interest flanked by ribozymes that undergo spontaneous autocatalytic cleavage. The resulting RNA contains 5′ and 3′ ends that are then ligated by the nearly ubiquitous endogenous RNA ligase RtcB. Using this approach, protein-binding RNA aptamers that otherwise have minimal effects in cells become potent inhibitors. Additionally, RNA-based biosensors can now be expressed at high levels and used to detect metabolite fluctuations in mammalian cells. Overall, this expression system enables RNA aptamers and RNA devices to be used as tools for manipulating proteins and imaging cellular processes in mammalian cells.

Results

Designing autocatalytic transcripts as ligation substrates. To stabilize RNA aptamers and devices in cells, we wanted to express them as circles. RNA circles are resistant to intracellular exonucleases since they lack a 5′ or 3′ end. Naturally occurring circular RNAs show half-lives that can be measured in days[13], demonstrating the stabilizing effect of circularization.

Endogenous RNA circularization is primarily a consequence of 'back-splicing' reactions in messenger RNA (mRNA)[14,15]. A second mechanism for RNA circularization occurs during transfer RNA (tRNA) splicing. A subset of tRNAs contain an intron that is cleaved by a tRNA-specific endonuclease[16]. The tRNA endonuclease creates unique ends on RNA: a 5′ hydroxyl and a 2′,3′-cyclic phosphate at the 3′ end[17,18]. These ends are recognized for ligation by RtcB[19]. After cleavage, RtcB ligates the resulting tRNA to form the mature tRNA[20–22].

Since the released intron also contains 5′ and 3′ ends that can be ligated by RtcB, the intron can be circularized (Supplementary Fig. 1a). By inserting the fluorogenic aptamer Broccoli[23] into the intron sequence of $tRNA^{Tyr}$, we previously showed that a circular Broccoli-containing intron was generated[24].

However, in this system, termed 'tricY', circular Broccoli levels were only slightly higher than those of linear Broccoli expressed from an identical U6 promoter[24]. Based on the high level of uncleaved linear tRNAs (Supplementary Fig. 1b,c), the rate-limiting step appears to be endonucleolytic cleavage to generate RNA fragments with RtcB-compatible ends (Supplementary Fig. 1c).

[1]Tri-Institutional PhD Program in Chemical Biology, Weill Cornell Medicine, The Rockefeller University, Memorial Sloan Kettering Cancer Center, New York, NY, USA. [2]Department of Pharmacology, Weill Cornell Medicine, Cornell University, New York, NY, USA. *e-mail: srj2003@med.cornell.edu

We therefore wanted to efficiently generate RNAs containing RtcB-compatible 5′ and 3′ ends within mammalian cells. To mimic processing by tRNA endonuclease, we considered expressing RNA transcripts containing ribozymes that autocatalytically cleave and produce the same 5′ hydroxyl and 2′,3′-cyclic phosphate ends as the tRNA endonuclease.

Most ribozymes show cleavage rates that require tens of minutes or even hours for the cleavage to reach completion under physiological conditions[25]. This would not be useful, since an expressed RNA would be degraded before the 5′ and 3′ ends are generated. However, recently described 'Twister' ribozymes[26] undergo self-cleavage to produce 5′ hydroxyl and 2′,3′-cylic phosphate ends at rates hundreds of times faster than optimized hammerhead ribozymes[27,28] under physiological conditions[29].

We reasoned that we could genetically encode RNAs containing a 5′ hydroxyl and a 2′,3′-cyclic phosphate by expressing RNAs of interest flanked by Twister ribozymes. After autocatalytic processing, the 5′ and 3′ ends would become substrates for RtcB-mediated ligation. Following ligation, the RNA between the ribozymes would be circularized.

In order to distinguish these circular RNA from others derived from back-splicing or tRNA introns, we termed circular RNAs generated in this manner as ribozyme-assisted circular RNA (racRNA) (Fig. 1). The intermediates required to generate racRNA are designated as primary racRNA (pri-racRNA) and pre-racRNA, which denote, respectively, the linear transcript that contains the ribozymes before cleavage and the linear transcripts that are cleaved but not yet circularized (Fig. 1).

Selection of ribozymes for RNA processing. We wanted to test different pairs of ribozymes to determine which combinations would efficiently process pri-racRNA to pre-racRNA. We first selected potential ribozymes for the 3′ end of the pri-racRNA. After cleavage, a 2′,3′-cyclic phosphate should remain on the pre-racRNA. Since it is important to leave as little residual ribozyme sequence as possible on the pre-racRNA after cleavage, we focused on ribozymes that cleave near its 5′ end, such as the hatchet ribozyme[30] and a type P1 Twister ribozyme (*Oryza sativa* Osa-1-4)[31].

We also selected potential ribozymes for the 5′ end of the pri-racRNA. These ribozymes should leave a 5′ hydroxyl on the pre-racRNA. To leave a minimal residual ribozyme sequence, we focused on ribozymes that cleave near its 3′ end, including a type P3 Twister from *Nematostella vectensis*[26], Twister Sister versions 3 and 4 (ref. [30]), the pistol ribozyme (M4 construct from *Lysinibacillus sphaericus*)[30] and a minimal type I hammerhead ribozyme[32].

We wanted the residual fragments remaining on the 5′ and 3′ ends of the RNA of interest to hybridize to each other in order to juxtapose the 5′ and 3′ ends in a way that resembles the physiological tRNA substrate for RtcB (Supplementary Fig. 1a). In tRNA, the 5′ and 3′ ends are presented at the ends of a base-paired stem. To mimic this stem in our RNAs, we designed the pre-racRNA so that the 5′ and 3′ ends came together to form a stem comprising 19 base pairs, as well as a 2 nt overhang on the 5′ end and a 7 nt overhang on the 3′ end. The four terminal base pairs of the stem and the overhangs are identical to the ends normally presented by the tyrosine tRNA, a natural substrate for RtcB[21] (Supplementary Fig. 2). In each tested construct, these 'stem-forming sequences' at the 5′ and 3′ ends were inserted between the internal cleavage site of each ribozyme and the RNA of interest (Supplementary Fig. 2).

To preserve the ribozymes' predicted secondary structure after introducing these stem-forming sequences, compensatory mutations were included in each ribozyme sequence (Supplementary Fig. 2). A variant of the P3 Twister was also generated that contains an altered 5′ stem-forming sequence (U2A) to preserve an adenosine that is normally found at this position in this ribozyme (Supplementary Fig. 2).

Next, we synthesized pri-racRNAs with various pairwise combinations of ribozymes by in vitro transcription. To facilitate visualization of the RNAs, we used the Broccoli aptamer, which is readily visualized in gels by staining with DFHBI-1T[6], a fluorophore that becomes fluorescent upon binding Broccoli[23]. In each construct, Broccoli was flanked by the different ribozymes. The cleavage of either or both ribozymes was assessed by examining the size of the RNA (Supplementary Fig. 3). In these experiments, the RNA was resolved by denaturing gel electrophoresis; the denaturant was washed out and the gel was stained with DFHBI-1T.

Comparison of different pairwise combinations of ribozymes demonstrated that cleavage at both the 5′ and 3′ sides of Broccoli was most efficient when the P1 Twister was at the 3′ end, especially when the 5′ ribozyme was a Twister Sister, Pistol ribozyme or the P3 Twister containing the U2A mutation (Fig. 2a and Supplementary Fig. 3). The hemi-cleaved RNA—RNA in which only the 5′ or 3′ ribozyme underwent cleavage—was present at low levels and did not accumulate (Fig. 2a, labeled as '5′- or 3′-cleaved').

We next confirmed that this autocatalytically processed pre-racRNA could be circularized by RtcB. Incubation of the pre-racRNA with RtcB from *Escherichia coli* resulted in a faster-migrating band (Fig. 2b), consistent with a known property of circular RNAs[33]. This effect was blocked by incubation of the pre-racRNA with T4 polynucleotide kinase (PNK), which was expected to generate a 5′ phosphate and convert the 2′,3′-cyclic phosphate to a 3′ hydroxyl[34,35]. Lastly, we treated the RNAs with RNase R, which degrades linear RNA but not circular RNA. Only the RtcB-incubated RNA was resistant to RNase R (Supplementary Fig. 4a).

Overall these data demonstrate an approach for designing transcripts that autocatalytically generate 5′ hydroxyl and 2′,3′-cyclic phosphate ends and can be circularized by RtcB.

Ribozyme-flanked transcripts are circularized in cells. We next tested whether ribozyme-flanked aptamers are circularized in cells. We expressed ribozyme-containing transcripts from a plasmid using a U6 promoter[5]. For each construct, we measured the level and size of Broccoli-containing RNA by resolving whole-cellular RNA using polyacrylamide gel electrophoresis (PAGE), followed by gel staining with DFHBI-1T. As a preliminary test to determine whether the RNA was circular, we used actinomycin D (actD), which blocks RNA transcription. Typically, linear RNA aptamers are completely lost after 6 h of actD treatment due to their rapid degradation[24]. In contrast, circular RNA aptamers should show no change in abundance with this treatment[24].

Transcripts containing a 5′ P3 Twister U2A and a 3′ P1 Twister showed the highest level of expression of a Broccoli-containing RNA with no detected side products (Fig. 2c and Supplementary Fig. 4b). The abundance of this RNA was unaffected by actD treatment, suggesting that it is a circular RNA.

We used several approaches to determine whether this abundant and stable Broccoli-containing RNA was a circular RNA. First, we gel purified the band and assessed its sensitivity to RNase R. In contrast to a linear RNA standard, this RNA was not susceptible to RNase R-mediated degradation (Supplementary Fig. 4c).

Second, we found that this stable Broccoli RNA exhibited different mobility in gels with different concentrations of polyacrylamide, which is characteristic of circular RNA[33,36,37] (Supplementary Fig. 5a).

Third, we site-specifically cleaved the RNA using RNase H; RNase H selectively cleaves RNA at sites that are hybridized to a complementary DNA oligonucleotide. If an RNA is linear, then RNase H produces two products; however, if an RNA is circular, then RNase H cleavage produces a single product (Fig. 2d). We expressed Broccoli using Tornado, and purified the resulting putative circular RNA. Incubation of this RNA with RNase H and a 15-nucleotide-long DNA oligonucleotide designed to hybridize to an internal

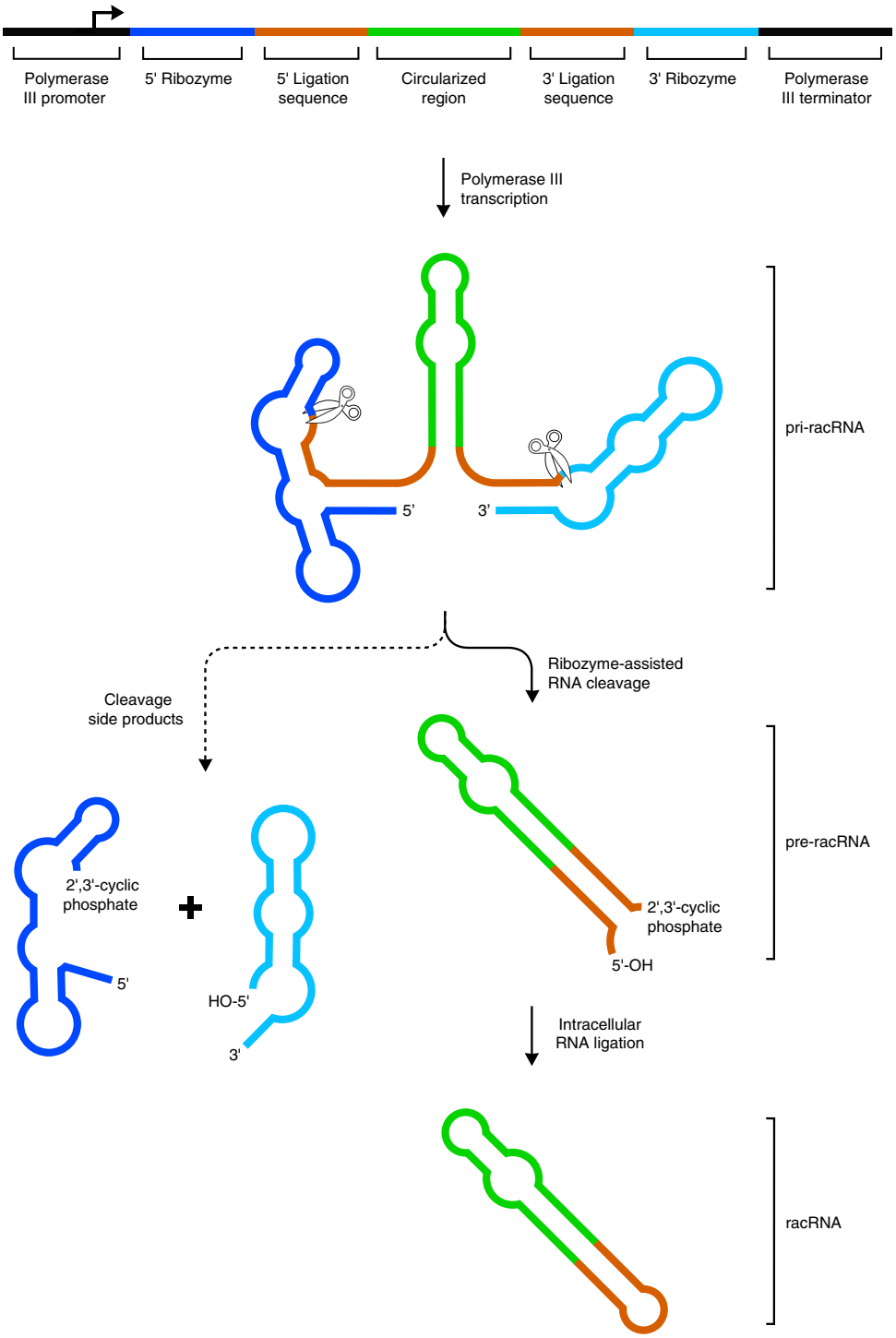

Fig. 1 | Conceptualization of an autocatalytic circular RNA mammalian expression vector. Construct design for autocatalytically processed circular RNA (circRNA) expression. The sequence that is expressed as a circular RNA (green) is flanked by the 5′- and 3′-stem-forming sequences (orange), each of which is flanked by the 5′- and 3′-self-cleaving ribozymes (blue and cyan, respectively). Once transcribed, this pri-racRNA becomes cleaved by each ribozyme, which generates a 2′,3′-cyclic phosphate and 5′-OH on the new RNA ends. The stem-forming sequences of the pre-racRNA hybridize and become circularized into racRNA by an endogenous RNA ligase before degradation. The unligated fragments of the pri-racRNA are rapidly degraded by exoribonucleases. Circular RNAs resist endogenous exoribonucleases, allowing the RNA aptamer to reach exceptionally high concentrations.

sequence generated a single RNA product. In contrast, a control linear RNA was cleaved into two fragments (Fig. 2d). Together, these experiments show that this stable Broccoli RNA is indeed circular and not merely an unusually stable linear RNA.

Next, we tested whether there is any heterogeneity at the ligation site in racRNAs. Sequencing of the gel-purified racRNAs showed that the ligation site consists of a single sequence (Supplementary Fig. 5b,c) dictated by the two ribozyme-cleavage sites (see Supplementary Fig. 2).

Since this type of racRNA was generated using two Twister ribozymes, we refer to the expression system that generated these circular RNAs as 'Tornado'.

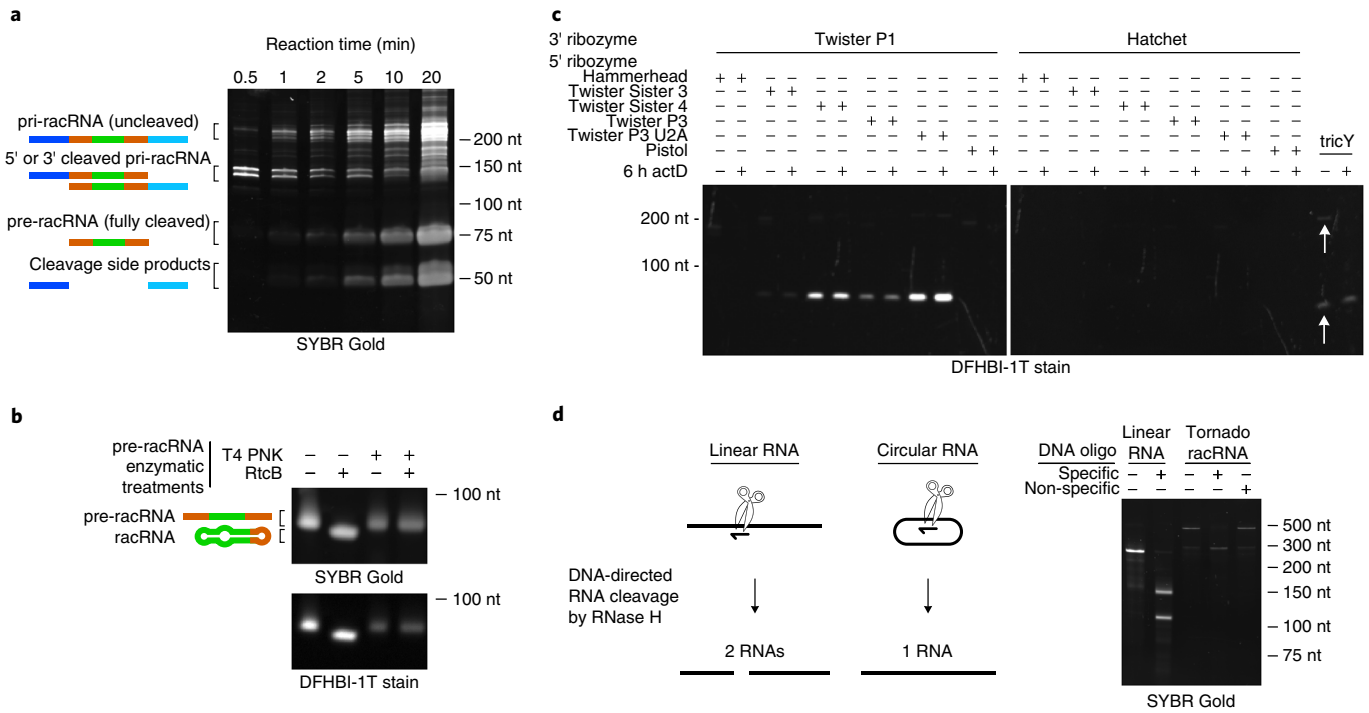

Fig. 2 | Tornado expression system generates circular RNA. a, Ribozymes efficiently self-cleave during transcription reactions. The construct containing Twister P1 and Twister P3 U2A ribozymes was transcribed in vitro and quenched with urea before running on denaturing PAGE and visualization of RNA. Fully cleaved products and the side products of cleavage accumulated efficiently and rapidly after transcription. **b**, Fully cleaved products of transcription in **a** contain appropriate ends for circularization by the endogenous ligase, RtcB. We excised the fully cleaved RNA from **a** and performed an RtcB ligation reaction. RtcB treatment produced a shift in gel mobility that was not observed without ligation or with pre-treatment with PNK. This shift in gel mobility suggests that the fully cleaved RNA contains the appropriate ends for ligation. Staining of the gel with DFHBI-1T and comparison of fluorescence relative to SYBR Gold signal demonstrated that circular Broccoli is brighter than linear Broccoli. **c**, Twister-based racRNA expression generated substantially higher levels of circular RNA than the previous circular RNA-expressing system. HEK293T cells expressed racRNA Broccoli from a variety of racRNA expression systems (see Fig. 1) with different combinations of 5′ and 3′ ribozymes, and were compared to expression using the tricY system. Cells were treated with actD for 6 h to observe the drop in RNA levels after inhibition of novel RNA synthesis. The Twister P1 and Twister P3 U2A construct, dubbed 'Tornado', expressed high levels of Broccoli RNA that exhibited high stability, characteristic of circRNA. **d**, Tornado-expressed RNA is decisively circular. DNA-directed cleavage by RNase H of a linear RNA produced two bands, each of expected size given the transcript length and probe site. The identical treatment of the same sequence expressed from Tornado produced a single band similar in size to the uncleaved transcribed sample.

Comparison of circular RNA expression methods. We next wanted to compare levels of racRNA generated by the Tornado expression system to other circular RNA expression methods. Expression of linear Broccoli in HEK293T cells produced very dim green fluorescence (Fig. 3a) at the short exposure time used in this experiment (200 ms). With the same U6 promoter and exposure time, fluorescence was slightly higher in cells expressing circular Broccoli using the tricY system (Fig. 3a). However, markedly higher levels of green fluorescence were detected when expressing circular Broccoli using the Tornado expression system (Fig. 3a). Notably, circular RNA was present in the cytoplasm but at much lower levels in the nucleus (Supplementary Fig. 6a). Quantification of fluorescence using flow cytometry indicated that cells expressing Broccoli using Tornado were nearly 200 times as bright as linear Broccoli-expressing cells (Supplementary Fig. 6b). These data support the idea that the Tornado expression system produces high levels of circular RNA.

An important question is whether aptamers are folded properly when expressed as a circular RNA. Since Broccoli needs to be folded to produce fluorescence, this experiment demonstrates that circularization does not impair the folding of this aptamer. Furthermore, in-gel fluorescence of linear and circular Broccoli bands suggests that circularization stabilizes the folded form of Broccoli, since Broccoli in a circular RNA exhibits ~50% more fluorescence than linear Broccoli (Fig. 2b).

To further test whether aptamers are folded when expressed using the Tornado system, we expressed Corn, a structurally distinct fluorogenic RNA aptamer that activates the yellow fluorescence of its cognate fluorophore (DFHO)[38]. Expression of Corn as a racRNA resulted in robust fluorescence (Fig. 3b) that was resistant to actD treatment (Supplementary Fig. 7). In contrast, Corn fluorescence was weakly detected when expressed as a linear RNA, and tricY-expressed Corn transcripts were not detected.

Notably, racRNA was expressed using the Tornado expression system in all mammalian cells tested (Fig. 3c,d). Thus, the Tornado expression system functions in different cell types and expresses diverse RNA aptamers in functional and folded conformations.

Next, we asked whether any other circular RNA expression system generates circular RNA at levels similar to those with the Tornado expression system. We tested systems previously shown to generate high levels of circular RNA, including the rearranged group-I-introns from phage T4 (ref. [39]), the 'sno-lncRNA' system, which generates nuclear-enriched circular introns[40] as well as the tricY system. We expressed circular Broccoli using each expression system in HEK293T cells. Total RNA was harvested, and Broccoli-containing RNA was either not detectable or was expressed at markedly lower levels than that seen with the Tornado system (Fig. 3e and Supplementary Fig. 4d). Thus, the Tornado expression system generates substantially higher levels of circular RNA than other expression systems.

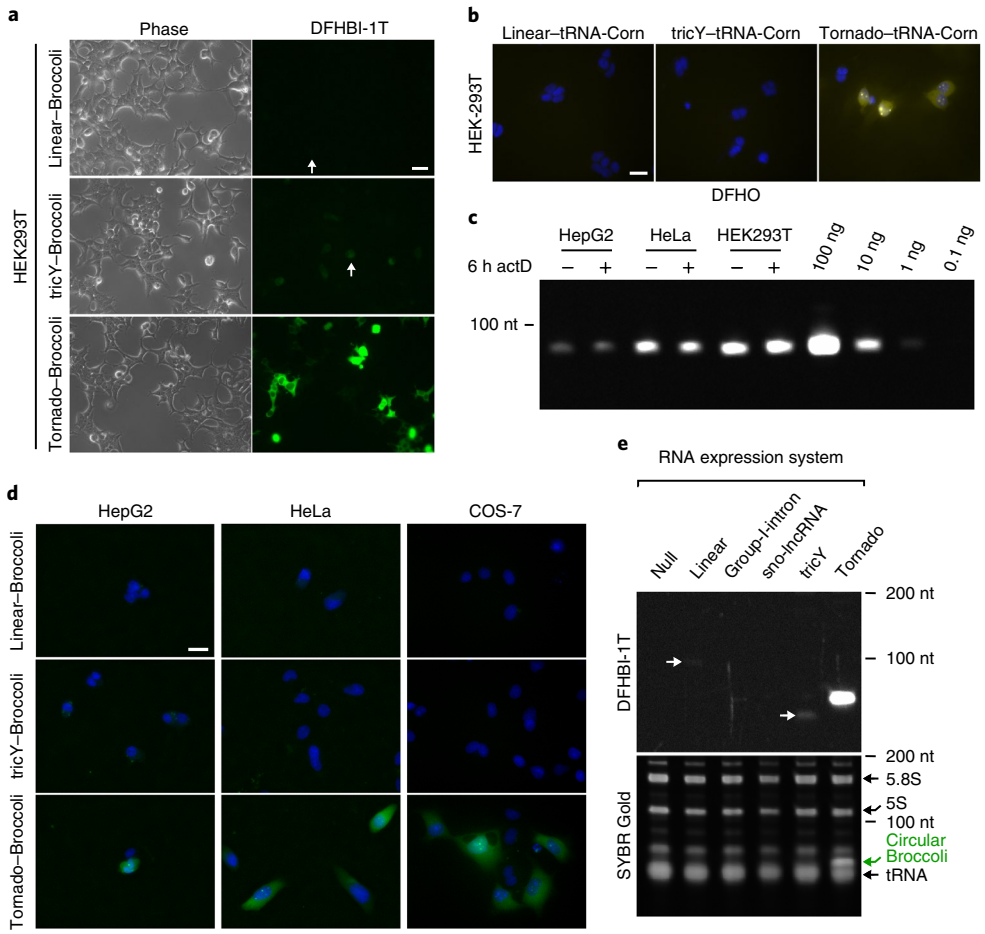

Fig. 3 | Abundant circRNA expression in different cell lines with fluorogenic aptamers. a, Broccoli was readily detected by fluorescence microscopy when expressed as a circular RNA using the Tornado expression system in HEK293T cells. At the same short exposure time, tricRNA Broccoli exhibited substantially lower fluorescence and linear Broccoli was barely detected. Representative cells showing fluorescence from linear or tricRNA Broccoli are highlighted with white arrows. Scale bar, 25 μm. **b**, The Tornado expression system enabled efficient expression of the Corn aptamer in a circular form. HEK293T cells expressing Corn in a tRNA scaffold using a linear promoter, the tricY system, and the Tornado expression system were imaged using fluorescence microscopy after incubation of cells with the Corn-binding fluorogenic dye, DFHO. Scale bar, 25 μm. **c**, Quantification of Tornado-expressed circular RNA concentration in transfected cells. After three days of expressing Broccoli using Tornado, total RNA from HepG2, HeLa and HEK293T cells was harvested and separated by 10% PAGE alongside circular Broccoli standards (100, 10, 1, 0.1 ng). Normalizing for transfection efficiency, intracellular circular Broccoli concentrations were estimated as 1.6 μM for HepG2, 16 μM for HeLa and 21 μM for HEK293T cells (see Methods). **d**, The Tornado expression system resulted in efficient circularization of an RNA aptamer in a variety of cell lines. Three days after transfection with plasmids encoding linear Broccoli or circular Broccoli with either the tricY system or the Tornado expression system, cells (HepG2, HeLa and COS-7) were imaged by fluorescence microscopy with DFHBI-1T. Cell nuclei are labeled with Hoechst stain. In all cell types observed, green fluorescence from Broccoli was readily detected only when expressed using the Tornado expression system. Scale bar, 25 μm. **e**, Tornado-expressed circular Broccoli is highly abundant. Broccoli was expressed using the Tornado expression system and other methods for generating circular RNA in HEK293T cells. After separation of total RNA on a 6% PAGE gel, Broccoli-containing RNAs were detected by a DFHBI-1T gel stain while total RNA was detected by SYBR Gold. Circular Broccoli bands were substantially increased when expressed using the Tornado expression system compared to all other methods. The Tornado-generated circular Broccoli band detected by SYBR Gold is as abundant as the 5.8S, 5S and tRNA bands.

Tornado racRNAs achieve micromolar concentrations. We found that the Tornado expression system can result in RNA expression that matches levels of endogenous, highly expressed small RNA. SYBR Gold staining of total cellular RNA from HEK293T cells showed the expected abundant cellular RNAs such as tRNA, 5S and 5.8S RNA (Fig. 3e). Notably, when total RNA was prepared from cells expressing Broccoli using the Tornado expression system, an additional band was detected at an intensity nearly equal to the 5.8S and 5S bands, and at an intensity greater than the tRNA bands. This band was clearly circular Broccoli, based on its mobility, staining with DFHBI-1T and its appearance only in cells transfected with the Tornado expression system. Thus, Tornado produces circular RNA that reaches levels similar to those of stable and highly expressed endogenous cellular RNAs.

In many cases, aptamers need to be expressed at levels comparable to protein expression levels to modulate that protein's function. The intracellular concentration of circular Broccoli was therefore determined by generating a standard curve using RtcB-circularized in vitro transcribed Broccoli standards (Fig. 3c). Lysates were prepared from a known number of cells, and the average intracellular volume of each cell line was calculated according to its diameter when in suspension (see Methods). Based on this analysis, circular Broccoli was 21 μM in HEK293T cells, 16 μM in HeLa cells and 1.6 μM in HepG2 cells. This indicates that racRNAs are expressed at levels that should saturate protein targets.

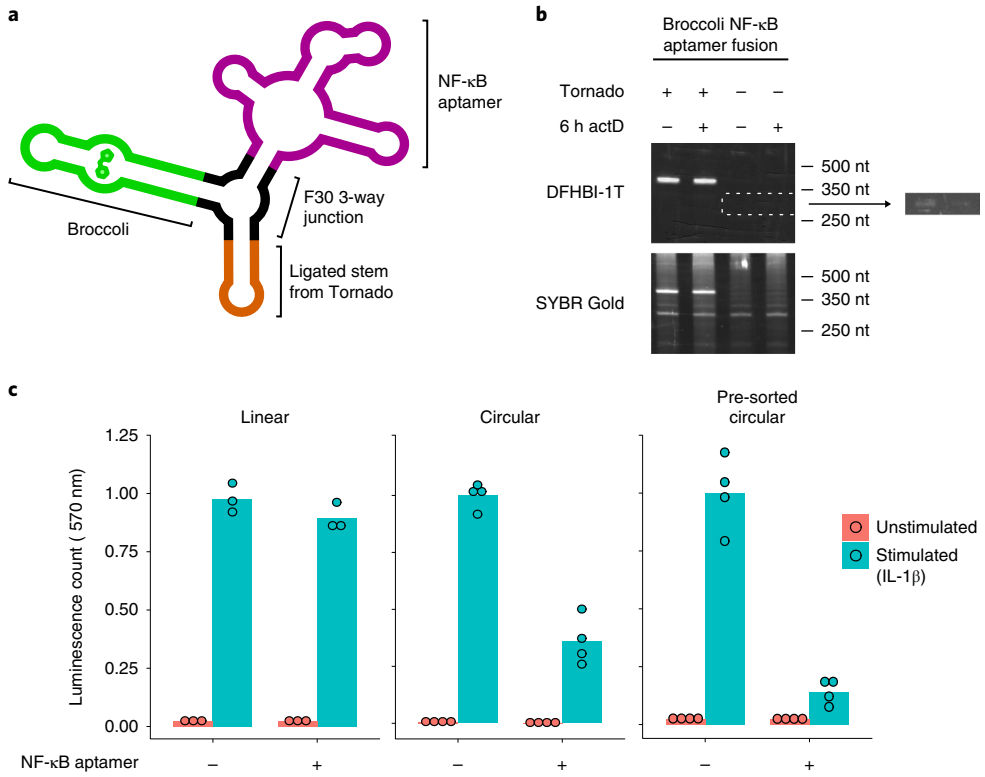

Fig. 4 | Improved inhibition of NF-κB pathway by circRNA aptamers. a, Design of circular RNAs that contain NF-κB pathway-inhibiting aptamers. Circular RNAs are designed to contain an F30 three-way junction (black) with Broccoli on one arm and an NF-κB aptamer on the other, while the circularizing stem forms at the base of the F30 three-way junction. This design allows for functional investigation of pathway-inhibiting aptamers while also probing for abundance of this circular RNA using Broccoli fluorescence. **b**, Tornado efficiently expresses the NF-κB aptamer as a racRNA in HEK293 cells. HEK293 cells were transfected with a plasmid expressing the NF-κB aptamer as either a linear RNA or racRNA for two days. Cells were then treated with actD for 6 h, and RNA was harvested to detect aptamer expression levels before and after actD treatment. Aptamer levels were detected based on in-gel staining using DFHBI-1T to detect Broccoli-containing RNA. Tornado-expressed racRNA generated a single, bright Broccoli fluorescent band that was resistant to actD treatment, while the linear band was barely detected (outlined in white and shown in a brightness-adjusted image on the right). **c**, The NF-κB aptamer is an effective pathway inhibitor when expressed using the Tornado expression system. IL-1β-induced NF-κB pathway activation was detected by luminescence in cells encoding luciferase driven by a NF-κB promoter. Cells expressed either the circular or linear NF-κB aptamer as indicated. IL-1β-induced luminescence is 8% inhibited by linear expression and 70% inhibited by circular expression. Circular RNA-expressing cells that were pre-sorted for aptamer expression based on their green fluorescence showed more efficient pathway inhibition (~85%). Luminescence was normalized according to the number of cells present during the assay. All signals were normalized to that of cells expressing RNA without the NF-κB aptamer after activation. Data in this panel represent the mean ($n = 3$ or 4 stimulation- and assay-independent samples).

racRNA expression is not cytotoxic. We next asked whether expression of circular RNAs using the Tornado expression system would cause cytotoxicity. Expression of Broccoli using the Tornado expression system elicited low levels of apoptosis, similar to expression of a linear mCherry mRNA, as measured by cleaved poly (ADP-ribose) polymerase (PARP) (Supplementary Fig. 8a). The cellular proliferation rate was also similar (Supplementary Fig. 8b).

Next, we determined whether the expression of circular Broccoli would activate an innate immunity response, as has been observed for circular RNAs of foreign origin[41]. We measured activation of the nuclear factor kappa-light-chain-enhancer of activated B cells (NF-κB) pathway and retinoic acid-inducible gene I (RIG-I) levels, which are elevated following activation of the innate immune pathway[42,43]. NF-κB pathway activation and RIG-I levels were not elevated following expression of circular Broccoli compared to those of the mCherry mRNA or linear Broccoli (Supplementary Fig. 9a,b). Overall, these data suggest that innate immune activation by racRNAs is negligible compared to conventional RNA expression systems.

Since racRNA biosynthesis may reduce the availability of RtcB, it is possible that RtcB-dependent tRNA maturation could be impaired. However, RNA blotting analysis showed minimal effects on the uncleaved:cleaved ratio of endogenous tRNA substrates of RtcB (Supplementary Fig. 10). Thus, the Tornado expression system does not affect these various measures of cytotoxicity and normal cell function.

Tornado improves the efficacy of protein-inhibiting aptamers. We asked whether expression of protein-binding aptamers using the Tornado system would render them effective protein-modulating agents. Several aptamers have been generated that bind the NF-κB protein monomers, p50 and p65 (refs. [44–46]), preventing their transcriptional activity[47]. These aptamers were expressed as circular RNAs that include the Broccoli aptamer (Fig. 4a) so that aptamer-expressing cells could be detected based on Broccoli fluorescence. Expression of these racRNAs was confirmed by stability to actD treatment (Supplementary Fig. 11a).

We next assessed whether racRNAs would inhibit NF-κB signaling. In these experiments, NF-κB was activated by application of interleukin (IL)-1β (50 ng ml^{-1}, 2.5 h) to HEK293 cells. Transcriptional activation was measured using a luciferase reporter (see Methods). In control cells expressing circular Broccoli RNA without the NF-κB aptamer, IL-1β induced robust

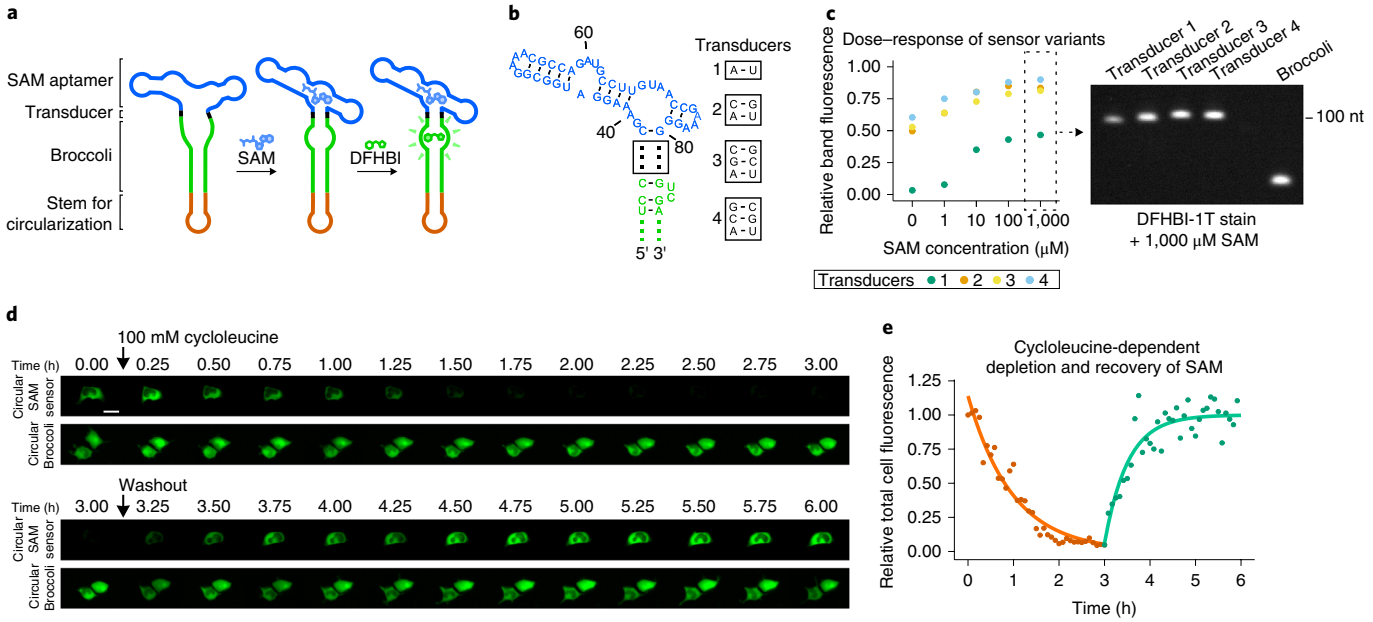

Fig. 5 | Dynamic SAM detection in mammalian cells by circRNA-based biosensors. a, Design of intracellular metabolite biosensors composed of circular RNA. Biosensors are designed so that Broccoli folds only when SAM binds to the SAM aptamer. SAM binding to its aptamer leads to folding of the aptamer and stabilization of the transducer stem. The stabilized transducer stem then facilitates Broccoli folding. The SAM biosensor was expressed using the Tornado expression system such that the circularizing stem would be located on the opposite end of Broccoli. This design is adapted from previously reported linear SAM biosensors[9]. **b**, Sequences of biosensor variants for biosensor optimization. The overall sequence and simplified structure of the SAM aptamer and transducer region are shown. Four different transducers were tested and the sequence of each is shown, boxed. **c**, In vitro optimization of the SAM biosensor's transducer stem for SAM detection. RNA from HEK293T cells expressing each biosensor variant using Tornado was harvested, resolved on a PAGE gel and then stained with DFHBI-1T to detect RNA bands corresponding to the SAM biosensor. Shown is quantified fluorescence after addition of the indicated concentrations of SAM to the staining solution. Band intensities were normalized to the brightness of the control Broccoli band on the right. Shown is an image of the gel stained with DFHBI-1T along with the highest SAM concentration (1,000 μM). The minimal transducer stem (Transducer 1) produced the greatest signal:noise ratio as measured by fluorescence in the presence and absence of SAM. **d**, Dynamic detection of intracellular SAM levels using the Tornado-expressed biosensor. HEK293T cells expressing the circular SAM biosensor or circular Broccoli were imaged after treatment with cycloleucine and after replacement of the media with cycloleucine-free media. Images are shown at 15 min intervals along with results for a representative fluorescent cell. Scale bar, 25 μm. **e**, Quantification of live-cell SAM levels based on biosensor fluorescence. Total cell fluorescence from the biosensor was quantified from **d** (see Methods) at 5 min intervals and plotted after normalization to the signal from a cell expressing circular Broccoli at the corresponding time points. SAM decay was observed following addition of cycloleucine (orange), and SAM recovery (green) is seen after withdrawal of cycloleucine.

luciferase activity (Supplementary Fig. 11b). This was inhibited by BAY 11-7082, an NF-κB pathway inhibitor[48]. One of the aptamers (variant 5), previously shown to bind to the p65 dimer with 11 nM affinity[45], strongly inhibited activation (~65%) (Supplementary Fig. 11b). Additionally, inhibition of pathway activation was diminished when this aptamer was replaced with a low-binding affinity mutant (Supplementary Fig. 11b). Thus, we proceeded with further experiments using this aptamer.

Next, we compared the activity of the NF-κB aptamer when expressed as either a linear RNA or a racRNA. The linear aptamer was degraded by actD and the Tornado-expressed aptamer was more abundant and stable (Fig. 4b). Expression of the linear aptamer inhibited pathway activation by only 8%, while the circular aptamer blocked 65% of activation (Fig. 4c). Additionally, after enriching for cells expressing the circular NF-κB aptamers by sorting transfected cells for Broccoli fluorescence, 85% of pathway activation was inhibited (Fig. 4c). We also observed that the circular aptamer was more folded than the linear aptamer using a B_{max} (maximum number of binding sites) calculation (Supplementary Fig. 12a,b). Thus, expression as racRNAs markedly improves the effectiveness of pathway-inhibiting aptamers.

Imaging of cellular metabolites using circular RNA. Genetically encoded biosensors can be developed using fluorogenic RNA aptamers such as Spinach and Broccoli. Typically, RNA-based biosensors are constructed by fusing an aptamer that binds the molecule of interest with the fluorogenic aptamer by a transducer stem. In this way, binding of the metabolite leads to folding and fluorescence of the fluorogenic aptamer[9].

Because RNA devices are highly unstable in mammalian cells, they have been used only in bacterial cells[49], many of which can contain high levels of T7 RNA polymerase, thereby ensuring high expression in the bacterial cytosol.

To test whether these RNA devices could be used in mammalian cells when circularized by the Tornado system, we expressed a SAM biosensor composed of Broccoli and a SAM-binding aptamer derived from a SAM riboswitch[9]. A linear biosensor with a similar sequence has previously been used in *E. coli*[9].

We designed the racRNA so that circularization would occur at the Broccoli base of the Broccoli–SAM aptamer fusion (Fig. 5a). Although the SAM biosensor was previously optimized in the context of a linear RNA[9], we re-optimized the biosensor in the circular RNA context to have the optimal signal relative to background. For these optimization experiments, we selected four transducers of variable length and sequence (Fig. 5b). These transducers were inserted between Broccoli and the SAM aptamer, expressed in cells and cellular RNA was harvested. Each of the transducer variants was expressed as a racRNA (Supplementary Fig. 13). The RNAs were resolved by gel electrophoresis, and both background and SAM-induced fluorescence were measured in the gel by sequentially adding increasing amounts of SAM to the DFHBI staining buffer (Fig. 5c). The biosensor containing the shortest transducer

(Transducer 1) exhibited the largest signal relative to background, high specificity and rapid kinetics of fluorescence activation by SAM (Supplementary Fig. 14a,b). Therefore, this biosensor was used for detection of SAM in all subsequent experiments.

Next, we expressed the optimized SAM biosensor in HEK293 cells both as a linear RNA and a racRNA. As expected, gel staining of whole-cell RNA showed substantially higher expression of the circular SAM biosensor than the linear biosensor (Supplementary Fig. 14c).

We then sought to determine whether the SAM biosensor would detect dynamic changes in SAM levels in HEK293 cells. We readily detected Broccoli fluorescence when the biosensor was expressed using Tornado. Cells expressing the linear biosensor had no detectable fluorescence at this exposure time (200 ms) (Supplementary Fig. 14d). Within 30 min after application of cycloleucine, a SAM biosynthesis inhibitor[50], the fluorescence of cells expressing the circular SAM biosensor was noticeably reduced, with a complete loss of fluorescence within 2 h (Fig. 5d). Cells expressing the Broccoli aptamer as a racRNA without the SAM aptamer showed no change in fluorescence following treatment with cycloleucine (Fig. 5d). Therefore, the reduction in fluorescence in cells expressing the SAM biosensor reflects a selective effect of cycloleucine on intracellular SAM levels rather than a non-specific effect on Broccoli fluorescence.

Next, we washed out the cycloleucine to determine whether the drop in intracellular SAM levels was reversible. Following replacement of the media with cycloleucine-free media, fluorescence levels rapidly increased to those observed at the beginning of the experiment (Fig. 5d). No change in fluorescence was observed in cells expressing racRNA Broccoli (Fig. 5d). This demonstrates that the Tornado expression system allows the SAM biosensor to accumulate to a level that is sufficient for imaging of metabolites in mammalian cells.

Discussion

Synthetic RNA biology entails the use of engineered RNA to manipulate and image cellular function. Because RNA aptamers and devices are highly unstable in mammalian cells, these tools are rarely used for synthetic biology applications in mammalian cells. We show that this problem is overcome by the Tornado expression system, which expresses RNA in the form of a circle without the need for co-expression of any proteins. The resulting circular RNAs are highly stable and achieve remarkably high expression levels in cells, comparable to those of proteins and the most abundant endogenous small RNAs in cells. The Tornado expression system involves expression of RNAs that contain Twister ribozymes flanking an RNA sequence of interest. This transcript autocatalytically processes itself to become a substrate for RtcB, an endogenous and nearly ubiquitous RNA ligase detected in nearly all animals, bacteria and archaea[20–22]. The RNA then undergoes end-to-end ligation, resulting in efficient expression of highly stable circular RNA.

Tornado-expressed racRNA aptamers show efficient inhibition of their target proteins. Additionally, RNA-based metabolite biosensors that could previously be used only in bacteria can now be used in mammalian cells to image metabolite dynamics. We expect that the Tornado expression system will readily facilitate the use of diverse aptamer technologies and RNA-based devices in mammalian cells.

Most endogenous circular RNAs are generated by back-splicing, a process that involves the mRNA splicing machinery[14,15]. In contrast, the Tornado expression system represents—to our knowledge—a previously unknown strategy for the generation of circular RNA.

Circularization is facilitated by hybridization of the pre-racRNA ends, which places the 5′ and 3′ ends near each other for RtcB-mediated ligation via a stem that forms by hybridization of the 5′ and 3′ ends of the pre-racRNA. The stem is designed to be relatively short, to prevent activation of endogenous double-stranded RNA-detection pathways. Expression of RNAs using the Tornado expression sequence will optimally contain this additional sequence, which facilitates RtcB-mediated ligation.

Although longer circular RNAs have been variably observed in the nucleus or cytoplasm[15,51,52], we readily detected racRNAs in the cytoplasm based on the fluorescence of the circular fluorogenic aptamers. The small size of racRNAs may allow them to pass through the nuclear pores and enter the cytoplasm. Thus, racRNA expression may be useful for manipulating or imaging cytosolic processes.

The Tornado expression system should enable the use of RNA-based tools generated by SELEX[1,2] to manipulate mammalian cells. The high levels of expression of circular RNAs using the Tornado expression system may render them especially effective for sponging microRNAs[53]. Since circular RNAs can be templates for translation in cells[54,55], the high level of expression described here may considerably enhance the protein synthesis levels achieved using this approach. For any circle synthesized using the Pol III promoter described here, internal U-rich Pol III termination sequences need to be avoided to ensure transcription of the full-length RNA.

Although the circular RNA expressed here did not exhibit cytotoxicity, circular RNAs that contain binding sites for an important RNA-binding protein or microRNA could elicit a cytotoxic response by sequestering these biomolecules. Although racRNAs could be used for therapeutic applications, further studies will be required to establish whether they exhibit toxicity in animals.

Online content

Any methods, additional references, Nature Research reporting summaries, source data, statements of data availability and associated accession codes are available at https://doi.org/10.1038/s41587-019-0090-6.

Received: 5 August 2018; Accepted: 1 March 2019;
Published online: 08 April 2019

References

1. Tuerk, C. & Gold, L. Systematic evolution of ligands by exponential enrichment: RNA ligands to bacteriophage T4 DNA polymerase. *Science* **249**, 505–510 (1990).
2. Ellington, A. D. & Szostak, J. W. In vitro selection of RNA molecules that bind specific ligands. *Nature* **346**, 818–822 (1990).
3. Rentmeister, A., Bill, A., Wahle, T., Walter, J. & Famulok, M. RNA aptamers selectively modulate protein recruitment to the cytoplasmic domain of β-secretase BACE1 in vitro. *RNA* **12**, 1650–1660 (2006).
4. Kahsai, A. W. et al. Conformationally selective RNA aptamers allosterically modulate the beta2-adrenoceptor. *Nat. Chem. Biol.* **12**, 1–11 (2016).
5. Good, P. et al. Expression of small, therapeutic RNAs in human cell nuclei. *Gene Ther.* **4**, 45–54 (1997).
6. Filonov, G. S., Kam, C. W., Song, W. & Jaffrey, S. R. In-gel imaging of RNA processing using broccoli reveals optimal aptamer expression strategies. *Chem. Biol.* **22**, 649–660 (2015).
7. Dittmer, P. J., Miranda, J. G., Gorski, J. A. & Palmer, A. E. Genetically encoded sensors to elucidate spatial distribution of cellular zinc. *J. Biol. Chem.* **284**, 16289–16297 (2009).
8. Paige, J. S., Wu, K. Y. & Jaffrey, S. R. RNA mimics of green fluorescent protein. *Science* **333**, 642–646 (2011).
9. Paige, J. S., Nguyen-Duc, T., Song, W. & Jaffrey, S. R. Fluorescence imaging of cellular metabolites with RNA. *Science* **335**, 1194 (2012).
10. Kellenberger, C. A., Wilson, S. C., Sales-Lee, J. & Hammond, M. C. RNA-based fluorescent biosensors for live cell imaging of second messengers cyclic di-GMP and cyclic AMP-GMP. *J. Am. Chem. Soc.* **135**, 4906–4909 (2013).
11. You, M., Litke, J. L. & Jaffrey, S. R. Imaging metabolite dynamics in living cells using a Spinach-based riboswitch. *Proc. Natl Acad. Sci. USA* **112**, E2756–E2765 (2015).
12. Litke, J. L., You, M. & Jaffrey, S. R. Developing fluorogenic riboswitches for imaging metabolite concentration dynamics in bacterial cells. *Methods Enzymol.* **572**, 315–333 (2016).

13. Ashwal-Fluss, R. et al. CircRNA biogenesis competes with pre-mRNA splicing. *Mol. Cell* **56**, 55–66 (2014).
14. Jeck, W. R. et al. Circular RNAs are abundant, conserved, and associated with ALU repeats. *RNA* **19**, 141–157 (2013).
15. Salzman, J., Gawad, C., Wang, P. L., Lacayo, N. & Brown, P. O. Circular RNAs are the predominant transcript isoform from hundreds of human genes in diverse cell types. *PLoS ONE* **7**, e30733 (2012).
16. Otsuka, A., de Paolis, A. & Tocchini-Valentini, G. P. Ribonuclease 'XlaI,' an activity from *Xenopus laevis* oocytes that excises intervening sequences from yeast transfer ribonucleic acid precursors. *Mol. Cell. Biol.* **1**, 269–280 (1981).
17. Laski, F. A., Fire, A. Z., RajBhandary, U. L. & Sharp, P. A. Characterization of tRNA precursor splicing in mammalian extracts. *J. Biol. Chem.* **258**, 11974–11980 (1983).
18. Filipowicz, W. & Shatkin, A. J. Origin of splice junction phosphate in tRNAs processed by HeLa cell extract. *Cell* **32**, 547–557 (1983).
19. Tanaka, N., Chakravarty, A. K., Maughan, B. & Shuman, S. Novel mechanism of RNA repair by RtcB via sequential 2′,3′- cyclic phosphodiesterase and 3′-phosphate/5′-hydroxyl ligation reactions. *J. Biol. Chem.* **286**, 43134–43143 (2011).
20. Popow, J. et al. HSPC117 is the essential subunit of a human tRNA splicing ligase complex. *Science* **331**, 760–764 (2011).
21. Tanaka, N. & Shuman, S. RtcB is the RNA ligase component of an Escherichia coli RNA repair operon. *J. Biol. Chem.* **286**, 7727–7731 (2011).
22. Englert, M., Sheppard, K., Aslanian, A., Yates, J. R. & Söll, D. Archaeal 3′-phosphate RNA splicing ligase characterization identifies the missing component in tRNA maturation. *Proc. Natl Acad. Sci. USA* **108**, 1290–1295 (2011).
23. Filonov, G. S., Moon, J. D., Svensen, N. & Jaffrey, S. R. Broccoli: Rapid selection of an RNA mimic of green fluorescent protein by fluorescence-based selection and directed evolution. *J. Am. Chem. Soc.* **136**, 16299–16308 (2014).
24. Lu, Z. et al. Metazoan tRNA introns generate stable circular RNAs in vivo. *RNA* **21**, 1554–1565 (2015).
25. Emilsson, G. M., Nakamura, S., Roth, A. & Breaker, R. R. Ribozyme speed limits. *RNA* **9**, 907–918 (2003).
26. Roth, A. et al. A widespread self-cleaving ribozyme class is revealed by bioinformatics. *Nat. Chem. Biol.* **10**, 56–60 (2014).
27. Khvorova, A., Lescoute, A., Westhof, E. & Jayasena, S. D. Sequence elements outside the hammerhead ribozyme catalytic core enable intracellular activity. *Nat. Struct. Biol.* **10**, 708–712 (2003).
28. De la Peña, M., Gago, S. & Flores, R. Peripheral regions of natural hammerhead ribozymes greatly increase their self-cleavage activity. *EMBO J.* **22**, 5561–5570 (2003).
29. Canny, M. D. et al. Fast cleavage kinetics of a natural hammerhead ribozyme. *J. Am. Chem. Soc.* **126**, 10848–10849 (2004).
30. Weinberg, Z. et al. New classes of self-cleaving ribozymes revealed by comparative genomics analysis. *Nat. Chem. Biol.* **11**, 606–610 (2015).
31. Liu, Y., Wilson, T. J., McPhee, S. A. & Lilley, D. M. J. Crystal structure and mechanistic investigation of the twister ribozyme. *Nat. Chem. Biol.* **7**, 1–7 (2014).
32. Uhlenbeck, O. C. A small catalytic oligoribonucleotide. *Nature* **328**, 596–600 (1987).
33. Tabak, H. F. et al. Discrimination between RNA circles, interlocked RNA circles and lariats using two-dimensional polyacrylamide gel electrophoresis. *Nucleic Acids Res.* **16**, 6597–6605 (1988).
34. Cameron, V. & Uhlenbeck, O. C. 3′-Phosphatase activity in T4 polynucleotide kinase. *Biochemistry* **16**, 5120–5126 (1977).
35. Das, U. & Shuman, S. Mechanism of RNA 2′,3′-cyclic phosphate end healing by T4 polynucleotide kinase-phosphatase. *Nucleic Acids Res.* **41**, 355–365 (2013).
36. Zaug, A. J. & Cech, T. R. The intervening sequence excised from the ribosomal RNA precursor of *Tetrahymena* contains a 5′-terminal guanosine residue not encoded by the DNA. *Nucleic Acids Res.* **10**, 2823–2838 (1982).
37. Ruskin, B., Krainer, A. R., Maniatis, T. & Green, M. R. Excision of an intact intron as a novel lariat structure during pre-mRNA splicing in vitro. *Cell* **38**, 317–331 (1984).
38. Song, W. et al. Imaging RNA polymerase III transcription using a photostable RNA-fluorophore complex. *Nat. Chem. Biol.* **13**, 1187–1194 (2017).
39. Ford, E. & Ares, M. Synthesis of circular RNA in bacteria and yeast using RNA cyclase ribozymes derived from a group I intron of phage T4. *Proc. Natl Acad. Sci. USA* **91**, 3117–3121 (1994).
40. Yin, Q. F. et al. Long noncoding RNAs with snoRNA ends. *Mol. Cell* **48**, 219–230 (2012).
41. Chen, Y. G. et al. Sensing self and foreign circular RNAs by intron identity. *Mol. Cell* **67**, 228–238.e5 (2017).
42. Yoneyama, M. et al. The RNA helicase RIG-I has an essential function in double-stranded RNA-induced innate antiviral responses. *Nat. Immunol.* **5**, 730–737 (2004).
43. Hornung, V. et al. 5′-Triphosphate RNA is the ligand for RIG-I. *Science* **314**, 994–997 (2006).
44. Lebruska, L. L. & Maher, L. J. Selection and characterization of an RNA decoy for transcription factor NF-κB. *Biochemistry* **38**, 3168–3174 (1999).
45. Wurster, S. E. & Maher, L. J. Selection and characterization of anti-NF-κB p65 RNA aptamers. *RNA* **14**, 1037–1047 (2008).
46. Wurster, S. E. & Maher, L. J. Selections that optimize RNA display in the yeast three-hybrid system. *RNA* **16**, 253–258 (2010).
47. Chan, R. et al. Co-expression of anti-NFκB RNA aptamers and siRNAs leads to maximal suppression of NFκB activity in mammalian cells. *Nucleic Acids Res.* **34**, 1–7 (2006).
48. Keller, S. A., Schattner, E. J. & Cesarman, E. Inhibition of NF-kappaB induces apoptosis of KSHV-infected primary effusion lymphoma cells. *Blood* **96**, 2537–2542 (2000).
49. Strack, R. L., Song, W. & Jaffrey, S. R. Using Spinach-based sensors for fluorescence imaging of intracellular metabolites and proteins in living bacteria. *Nat. Protoc.* **9**, 146–155 (2013).
50. Lombardini, J. B. & Talalay, P. Formation, functions and regulatory importance of *S*-adenosyl-l-methionine. *Adv. Enzyme. Regul.* **9**, 349–384 (1971).
51. Zhang, Y. et al. Circular intronic long noncoding RNAs. *Mol. Cell* **51**, 792–806 (2013).
52. Li, Z. et al. Exon-intron circular RNAs regulate transcription in the nucleus. *Nat. Struct. Mol. Biol.* **22**, 256–264 (2015).
53. Hansen, T. B. et al. Natural RNA circles function as efficient microRNA sponges. *Nature* **495**, 384–388 (2013).
54. Chen, C. Y. & Sarnow, P. Initiation of protein synthesis by the eukaryotic translational apparatus on circular RNAs. *Science* **268**, 415–417 (1995).
55. Wang, Y. & Wang, Z. Efficient backsplicing produces translatable circular mRNAs. *RNA* **21**, 172–179 (2015).

Acknowledgements

We thank J. D. Moon and H. Kim of the Jaffrey laboratory for comments and suggestions. This work was supported by NIH grant no. R01NS064516 (to S.R.J.) and by NIH fellowship no. F31AI134100 (to J.L.L.). Fluorescence-assisted cell-sorting experiments reported in this publication were supported by the Office of the Director of the National Institutes of Health under award no. S10OD019986 to Hospital for Special Surgery.

Author contributions

S.R.J. and J.L.L. conceived and designed the experiments. J.L.L. carried out experiments and analyzed data. S.R.J. and J.L.L. wrote the manuscript.

Competing interests

S.R.J, J.L.L. and Weill Cornell Medicine have filed a patent application covering aspects of this technology. S.R.J. is a co-founder of Lucerna Technologies and has equity in this company. Lucerna has licensed commercialization of technology related to Spinach and other RNA–fluorophore complexes.

Additional information

Supplementary information is available for this paper at https://doi.org/10.1038/s41587-019-0090-6.

Reprints and permissions information is available at www.nature.com/reprints.

Correspondence and requests for materials should be addressed to S.R.J.

Publisher's note: Springer Nature remains neutral with regard to jurisdictional claims in published maps and institutional affiliations.

© The Author(s), under exclusive licence to Springer Nature America, Inc. 2019

Methods

Preparation of RNA and observation of ribozyme cleavage. Double-stranded DNA for in vitro transcription was prepared from single-stranded DNA templates (Integrated DNA Technologies) and designed to contain a 5′ T7 promoter. Templates were amplified by PCR using *Taq* DNA polymerase (New England Biolabs, no. M02373) or Phusion High-Fidelity DNA Polymerase (New England Biolabs, no. M0530) and checked for quality by 0.8% agarose gel electrophoresis. Impure reaction products were isolated by gel excision and purified with the Qiaquick Gel Extraction kit (Qiagen, no. 28704). Pure PCR reactions were purified with the Qiaquick PCR purification kit (Qiagen, no. 28104).

In vitro transcription reactions using the AmpliScribe T7-Flash transcription kit (Lucigen, no. ASF3507) were carried out at 37 °C. For observation of ribozyme cleavage, transcription reactions were quenched by the addition of PAGE sample buffer containing urea (ThermoFisher, No. LC6876). Samples were separated using a precast 6% Tris-borate-EDTA (TBE)-urea gel (Life Technologies, no. EC68655), and run at 270 V in TBE buffer until completion. After staining with SYBR Gold (ThermoFisher, no. S11494) diluted 1:10,000 in TBE buffer, RNA bands were imaged using a ChemiDoc MP (Bio-Rad) with a preset channel (302 nm excitation and 590/110 nm emission).

All other transcription reactions for preparation of RNA were incubated overnight. Reactions were treated with RNase-Free DNase I (Lucigen, no. ASF3507) at 37 °C for at least 30 min to remove DNA templates, and then with 13.3 mM EDTA free of RNases (Sigma Aldrich, no. 03690) and incubated at 75 °C for 10 min. RNA was then purified from reactions using the RNA Clean & Concentrator kit (Zymo Research, no. R1015).

Excision and purification of RNA. After staining of PAGE gels, individual RNA bands were isolated from the gel. Bands were excised from gels and crushed by spinning through Gel Breaker tubes (IST Engineering, Inc., no. 3388-100). Samples were incubated in an extraction buffer (10 mM Tris-HCl, pH 6.8, 300 mM NaCl, 1 mM EDTA, prepared at room temperature) for 1 h at 25 or 37 °C and, after placing samples on dry ice briefly to freeze, they were incubated for an additional 1 h. Remaining gel pieces were removed through Costar SpinX columns (Corning, no. 8161), which was followed by ethanol precipitation.

Reactions of RNA templates with T4 PNK and RtcB. After gel purification of autocatalytically cleaved RNA, 300 pmol were treated with T4 PNK (New England Biolabs, no. M0201) according to the manufacturer's protocol at 37 °C for 30 min and inactivated for 20 min at 65 °C. The products were cleaned by phenol chloroform extraction using heavy phase-lock tubes (Quantabio, no. 2302830). Next, 10 pmol of either this purified T4 PNK-treated RNA or gel-purified RNA was ligated using RtcB Ligase (New England Biolabs, no. M0458) for 1 h at 37 °C.

Cloning of autocatalytic circRNA constructs. DNA templates containing Broccoli and each of the ribozyme combinations were prepared as described above, with flanking SalI and XbaI restriction sites. Designed using SnapGene software (GSL Biotech), these constructs were cloned downstream of a U6+27 promoter and upstream of the U6 terminator in a pAV vector containing the SV40 origin[56]. This U6 promoter includes the first 27 nucleotides of U6 RNA as described previously. Subsequent plasmids were made in the same way for cloning of one or two aptamers directly into the Tornado expression cassette at NotI and SacII, RsrII or KflI restriction enzyme sites. A gene for mCherry fluorescent protein expression was introduced into the backbone of this vector.

Cell culture and transfection. HEK293T/17 (ATCC CRL-11268), COS-7 (ATCC CRL-1651), HepG2 (ATCC HB-8065) and HeLa (ATCC CCL-2) cells were maintained in ×1 DMEM (Life Technologies, no. 11995-065) with 10% fetal bovine serum (FBS), 100 U ml^{-1} penicillin and 100 µg ml^{-1} streptomycin under standard tissue culture conditions. NF-κB reporter (luciferase) HEK293 (BPS Biosciences, no. 60650) cells were maintained in these conditions with 50 µg ml^{-1} hygromycin B (Life Technologies, no. 10687010). All cells were split using TrypLE Express (Life Technologies) according to the manufacturer's instructions.

Cell lines were plated for transfection using FuGENE HD (Promega, no. 2311), according to the manufacturer's instructions, with OptiMEM I Reduced Serum Media (ThermoFisher, no. 31985).

For experiments testing the stability of circRNAs, 5 µg ml^{-1} actD (Sigma Aldrich, no. A9415) was added to cells for 6 h before extraction of RNA.

RNA extraction. RNA was harvested from cultured cells by removing media and detaching enzymatically or directly lifting cells with ×1 phosphate buffered saline (PBS) (ThermoFisher, no. 10010031). Cell suspensions were mixed with TRIzol LS Reagent (Invitrogen, no. 10296010), then frozen and stored at −20 °C or purified immediately according to the manufacturer's instructions.

Total RNA concentrations were normalized using a NanoDrop 2000 (Thermo Scientific).

In-gel Broccoli imaging. Total RNA (1.0–2.5 µg) was separated using precast 6% or 10% TBE-Urea Gels (Life Technologies, no. EC68655), and run at 270 V in TBE buffer until completion. Gels were washed and probed for Broccoli as previously described[57], using minimal volumes (15 ml) to reduce escape of RNA from the gel. Gels were washed 3 × 5 min with water and then stained for 30 min in 10 µM DFHBI in buffer prepared at room temperature containing 40 mM HEPES, pH 7.4, 100 mM KCl and 1 mM $MgCl_2$. Broccoli bands were then imaged using a ChemiDoc MP (Bio-Rad) with 470/30 nm excitation and 532/28 nm emission. Gels were washed additionally with water and stained with SYBR Gold (ThermoFisher, no. S11494) diluted in TBE buffer. RNA bands were then imaged using a ChemiDoc MP (Bio-Rad) with a preset channel (302 nm excitation and 590/110 nm emission). Gel band intensities were quantified in Image Lab 5.0 software (Bio-Rad).

Reactions of circRNA with exoribonuclease. RNA was treated with T4 PNK or RtcB as described above. Products were purified using phenol chloroform extraction as described above. Purified reactions were treated with RNase R (Lucigen, No. RNR07250) as recommended by the manufacturer.

Site-specific circRNA cleavage. We designed a construct using Tornado that would express a 275 nt circRNA containing a series of scrambled RNA sequences as well as Broccoli. We transfected this plasmid into HEK293T cells, then extracted the RNA and purified the band where we observed in-gel Broccoli fluorescence, as described above. We prepared a sample of linear RNA with the same sequence by in vitro transcription and column purification. We also designed a 15 nt antisense DNA primer (Integrated DNA Technologies) with reverse complementarity for a region of the scrambled RNA sequence. Site-specific cleavage was performed in reactions containing 100 ng of the target RNA, 10 pmol of the antisense primer, RNasin ribonuclease inhibitor (Promega, no. N211A) and 0.5 µl Hybridase thermostable RNase H (Lucigen, no. H39500) in a total volume of 10 µl. Reaction buffer contained 100 mM NaCl, 40 mM Tris-HCl, pH 7.7, 4 mM $MgCl_2$, 1 mM dithiothreitol and 0.03% bovine serum albumin (BSA) prepared at room temperature. Reactions were incubated at 50 °C for 10 min before addition of Hybridase. Reactions proceeded for 2 h at 42 °C.

Sequencing of expressed racRNAs. RacRNAs were harvested from HEK239T cells with TRIzo LS Reagent (Invitrogen, no. 10296010) and purified by excision from denaturing acrylamide gels. Isolated RNAs were reverse transcribed using SuperScript III (ThermoFisher, no. 18080093) and subsequently amplified by *Taq* DNA polymerase (New England Biolabs, no. M02373) using convergent primers. Amplified DNA was visualized as a ladder of bands on agarose gels, and specific bands were excised (see Supplementary Fig. 7a). Excised DNA was cloned by TA cloning into the vector pCR4-TOPO (ThermoFisher, no. K457502), and individual clones were sequenced.

Microscopy and image processing. For imaging of cells, we used either pre-coated 3.5 cm glass-bottom dishes (MatTek Corporation, no. P35GC-1.5-14-C) or glass-bottom 24-well plates 1.5 (MatTek Corporation, no.P24G-1.5-13-F) that were coated with poly-D-lysine (Cultrex, No. 3429-100-01) for at least 3 h and rinsed twice in ×1 PBS. For cells that required imaging of longer than a few hours, these plates and dishes were additionally coated with Cultrex mouse laminin I (ThermoFisher, no. 50948048) for at least 1 h and rinsed twice in ×1 PBS. Cells were subcultured onto glass-bottom vessels 1–2 days after transfection, depending on the experiment. Thirty minutes before imaging, the medium was changed to FluoroBrite medium (ThermoFisher, no. A1896701) containing 40 µM DFHBI-1T or DFHO (synthesized[38] or Lucerna, no. 500-1mg) and 0.1 µg ml^{-1} of Hoechst 33342 (ThermoFisher, no. H3570). Live cell fluorescence images were obtained with a CoolSnap HQ2 CCD camera through a ×20 or ×40 air objective mounted on a Nikon Eclipse TE2000-E microscope and analyzed with NIS-Elements software. Conditions were maintained at 37 °C and 5% CO_2. The filter set used for Broccoli detection was a filter cube with excitation filter 470 ± 20 nm, dichroic mirror 495 nm (long pass) and emission filter 525 ± 25 nm. mCherry was detected using a 560 ± 20 nm excitation filter, 585 nm (long pass) dichroic mirror and 630 ± 37.5 nm emission filter. For Corn detection we used a filter cube with excitation filter 500 ± 12 nm, dichroic mirror 520 nm (long pass) and emission filter 542 ± 13.5 nm. Hoechst-stained nuclei were imaged with a 350 ± 25 nm excitation filter, 400 nm dichroic mirror (long pass) and 460 ± 25 nm emission filter (all filters provided by Chroma Technology). Exposure times: 200–500 ms for Broccoli, 200 ms for mCherry and Hoechst. Total cell fluorescence was computed using ImageJ by measuring the total signal in a cell's area and subtracting the background, which was measured by multiplying this area by the average background of an untransfected cell.

Flow cytometry comparing Broccoli-expressing cells. Three days after transfection, HEK293T cells were harvested and resuspended in 4% FBS/×1 PBS containing 40 µM DFHBI-1T and kept on ice till analysis. Cells were analyzed using a LSRFortessa (BD Biosciences). Populations of cells were gated to avoid cell doublets detected by forward and side scattering, followed by gating for live cells by DAPI fluorescence (355 nm excitation and 450/50 nm emission). Untransfected cells were used as a negative control for gating of Broccoli fluorescence (488 nm excitation and 530/30 nm emission). Plots were generated using FlowJo software (Tree Star, Inc.).

Comparison of Tornado to other circular RNA expression methods. Broccoli was cloned into other circular RNA-generating expression systems. The permuted-intron-exon system based on group I intron splicing was derived from the td T4 bacteriophage gene as previously described[39,58] and driven by the U6+27 promoter. Plasmids generating spliced sno-lncRNA containing Broccoli[40] and tRNA intron circular RNA containing Broccoli[24] were prepared as described previously.

Quantification of intracellular RNA concentrations. HepG2, HeLa and HEK293T cells were transfected with a plasmid encoding Tornado expression of Broccoli and a pSuperior plasmid for mCherry expression in a 1:1 ratio. After 2 days, cells were suspended using TrypLE. Each cell type was plated for imaging so that transfection efficiency could be quantified by red fluorescence the next day. For each cell suspension, the diameter and cell quantity in each cell line were quantified and then total RNA was extracted from each using TRIzol LS as described above. We calculated the gross intracellular volume of each sample based on quantification of cell number and diameter (13 µm for 293T, 20 µm for HeLa and 18 µm for HepG2). The average cellular volume was calculated using the formula for spherical volume. We then ran 1 µg of each cell line's total RNA by 10% denaturing PAGE and imaged Broccoli fluorescence in the gel using DFHBI-1T as described above. We quantified the amounts of circular Broccoli loaded on the gel by loading an in vitro circularized racRNA standard (0.01–100 ng) of the same sequence in adjacent lanes. We then calculated the gross amounts of circular Broccoli for each sample and calculated intracellular concentration. Lastly, we corrected our concentration values for transfection efficiency observations made in each cell line.

Immunoblots for detection of apoptosis and innate immune response in cells. For detection of apoptosis, HeLa cells were either treated with 1 µg ml^{-1} doxorubicin (Sigma Aldrich, no. D1515) 24 h before lysis or transfected using FuGENE HD (Promega, no. 2311) 48 h before lysis. For detection of innate immune response, HeLa cells were transfected with plasmids or RNA using Lipofectamine 3000 (ThermoFisher, no. L300001) 16 h before lysis. Cells were lysed in RIPA buffer (50 mM Tris-HCl, pH 7.4, 150 mM NaCl, 0.1% Triton X-100, 0.5% sodium deoxycholate, 0.1% sodium dodecyl sulfate, 1 mM sodium othovandate, 1 mM NaF, prepared at room temperature) containing Halt protease and phosphatase inhibitor cocktail (ThermoFisher, no. 78440) and quantified using a Pierce BCA Protein Assay Kit (ThermoFisher, no. 23225). Proteins were separated by PAGE, transferred to polyvinylidene difluoride membranes and blocked using 5% milk in TBS-T for 1 h at room temperature. For probing apoptosis and innate immune response, blots were incubated overnight in TBS-T containing 5% BSA at 4 °C with Cleaved PARP (Asp214) XP rabbit mAb (Cell Signaling Technology, no. D64E10) and Rig-I rabbit mAb (Cell Signaling Technology, no. D14G6), respectively. Control blots were incubated with GAPDH mouse mAb (Cell Signaling Technology, no. 97166). Blots were then probed using HRP-linked mouse IgG anitbodies (GE Healthcare, no. NA931V) or rabbit IgG (GE Healthcare, no. NA9314V) as secondary antibodies, developed using Pierce ECL Substrate (ThermoFisher, no. 32106) and signal was detected using a ChemiDoc MP (Bio-Rad).

Measurement of cell proliferation rates. HEK293T cells were independently transfected with plasmids encoding Broccoli using Tornado or encoding mCherry with FuGENE HD (Promega, no. 2311). Two days after transfection, cells were subcultured 1:4 and 1:8 onto glass-bottom plates (MatTek Corporation, no. P24G-1.5-13-F). The next day, fluorescent cells in each 1:4 subculture were counted in four fields, as well as the number of Hoechst-stained cells. After 2 days, the 1:8 subcultures were imaged in the same way. We calculated the number of non-fluorescent cells in each culture and then quantified doubling times of fluorescent and non-fluorescent cells according to the formula for exponential growth.

RNA blot measurements. RNA was harvested from cells using TRIzol LS Reagent (Invitrogen, no. 10296010) and separated by a denaturing 10% acrylamide gel. After overnight transfer to Hybond-N+ Membranes (GE Healthcare, no. RPN1210B), endgogenous tRNA^{Tyr} was probed by a biotin-labeled DNA probe complementary to the 5′ of mature tRNA^{Tyr} (Integrated DNA Technologies). Biotin signal was developed on the membranes using the Chemiluminescent Nucleic Acid Detection Module Kit (ThermoFisher, no. 89880).

Stimulation and detection of NF-κB signaling. HEK293 recombinant cells containing a NF-κB promoter-driven luciferase reporter (BPS Sciences, no. 60650) were used to detect activation of the NF-κB pathway. Two days after plasmid transfection, cells were transferred to 96-well plates in triplicate for luminescence detection. The next day, we stimulated cells and detected their activation. Chemically inhibited cells were incubated with 50 µM BAY 11-7082 (Santa Cruz Biotechnology, no. sc-200615) for 30 min. Cells were stimulated with 50 ng ml^{-1} recombinant human IL-1β (Peprotech, no. 200-01b) for 2.5 h. Luminescence was generated with the One-Glo luciferase assay system (Promega, no. E6110) as recommended by the manufacturer and detected at 570 nm (Molecular Devices SpectraMax L microplate reader).

Electrophoretic mobility shift assay for aptamer binding. Binding of NF-κB aptamers with p65 was detected by electrophoretic mobility shift assay. Samples (15 ul) containing 11 nM of linear or circular NF-κB and Broccoli fusions were prepared with 20 mM Tris-HCl, pH 8.0, 50 mM NaCl, 1 mM $MgCl_2$, 10 U RNaseOUT (Invitrogen, No. 10777-019, prepared at room temperature), 30 ng µl^{-1} yeast tRNA, 0.25 µg µl^{-1} BSA, 1 mM dithiothreitol and 5% glycerol. Samples were titrated with recombinant p65 (OriGene Technologies, No. TP320780) from 0.5 to 763 nM. After separation on a 5% polyacrylamide gel containing ×0.25 TBE, RNA was transferred to Hybond-N+ Membranes (GE Healthcare, no. RPN1210B) and subsequently treated with 50 µg mL^{-1} Proteinase K solution, RNA grade (Thermo Fisher, no. 25530049) in ×1 PBS for 1.5 h. Broccoli-containing RNA was detected by hybridization with DNA probes end-labeled by T4 PNK (New England Biolabs, no. M0201) with ATP, (γ-^{32}P) (PerkinElmer, no. BLU503H) and purified using illustra Microspin G-25 Columns (GE Healthcare, no. 27-5325-01). Bands were visualized using a Typhoon Trio (GE Healthcare) and quantified with ImageJ software before linearizing binding curves into Scatchard plots.

Fluorescence-assisted cell sorting of mammalian cells. HEK293 recombinant cells containing a NF-κB promoter-driven luciferase reporter (BPS Sciences, no. 60650) were used to detect NF-κB pathway activation. Forty-eight hours after transfection, cells were resuspended in a 4% FBS/×1 PBS solution containing 40 µM DFHBI-1T and kept on ice until analysis on a BD Influx Cell Sorter (BD Biosciences). With untransfected cells as a negative control for Broccoli fluorescence, transfected cells were analyzed and sorted based on their green fluorescence (488 nm excitation and 525 ± 50 nm emission). Processing and analysis of the data was performed in the FlowJo program (Tree Star, Inc.).

Circular SAM biosensor design and in-gel activation. The previously described SAM biosensor uses Spinach, which was replaced with Broccoli, since that is predicted to have a similar overall structure with improved folding in cells[23]. Transducer variants of Broccoli–SAM aptamer fusions were cloned into the pAV-U6+27-Tornado vector for circRNA expression. Two days after transfection of these plasmids and the plasmid for circular Broccoli into HEK293T cells, actD was added to cells, which were then harvested and the RNA extracted as described above. Isolated RNAs from cells treated or untreated with actD were separated using a 6% or 10% denaturing polyacrylamide gel, and the gels were imaged using DFHBI-1T followed by SYBR Gold staining.

We detected activation of biosensor fluorescence in a polyacrylamide gel by first staining with standard fluorescence buffer (10 µM DFHBI-1T, 40 mM HEPES, pH 7.4, 100 mM KCl, 1 mM $MgCl_2$) prepared at room temperature. After imaging, we then added 1 µM SAM (Sigma Aldrich, no. A7007) to the imaging buffer, stained the gels for an additional 30 min and imaged the signal again. This was repeated three more times after progressively adjusting SAM concentrations to 10, 100 and 1,000 µM. Transducer variant signals were compared at each concentration after normalization to the signal for circular Broccoli in each image.

Intracellular SAM imaging and quantification. HEK293T cells were transfected with Tornado plasmids encoding either the circular SAM biosensor with transducer 1 or circular Broccoli. Two days later, these cells were subcultured onto coated glass-bottom plates (MatTek Corporation, no. P24G-1.5-13-F) and imaged the next day. Using the live cell conditions described above, we imaged cells before and for 3 h after addition of cycloleucine (Sigma Aldrich, no. A48105) to 100 mM at 5 min intervals. Then, we withdrew cycloleucine and continued to image cells every 5 min for three additional hours. ImageJ[59] was used for processing images and for measurement of total cell fluorescence at each time point.

Fluorescence measurements of biosensor fluorescence in vitro. Biosensor RNA was transcribed in vitro using the AmpliScribe T7-Flash transcription kit (Lucigen, no. ASF3507) as describe above. RNAs were column purified and diluted to 1 µM in a buffer prepared at room temperature containing 10 µM DFHBI-1T, 100 mM KCl, 0.2 mM $MgCl_2$ and 40 mM HEPES, pH 7.4. SAM, *S*-adenosyl homocysteine, adenosine or methionine (all from Sigma Aldrich) were added to samples at 100 µM and fluorescence signal was measured at room temperature using a Fluoromax-4C (Horiba Scientific) with 470 nm excitation and 505 nm emission, 5 nm slit width and 0.1 s integration time.

To measure biosensor activation rate, the biosensor RNA was prepared to 1 µM in a buffer containing 10 µM DFHBI-1T, 100 mM KCl, 5 mM $MgCl_2$ and 40 mM HEPES, pH 7.4 in a constantly stirred cuvette at 37 °C. Fluorescence was collected by kinetics acquisition with 0.2 s integration time and, after 1 min of collecting background signal, 100 µM of SAM was quickly added to the cuvette.

Reporting Summary. Further information on research design is available in the Nature Research Reporting Summary linked to this article.

Data availability

All data supporting the findings of this study are available within the paper and its Supplementary Information files.

References

56. Paul, C. P., Good, P. D., Winer, I. & Engelke, D. R. Effective expression of small interfering RNA in human cells. *Nat. Biotechnol.* **20**, 505–508 (2002).
57. Filonov, G. S. & Jaffrey, S. R. RNA imaging with dimeric broccoli in live bacterial and mammalian cells. *Curr. Protoc. Chem. Biol.* **8**, 1–28 (2016).
58. Umekage, S. & Kikuchi, Y. In vitro and in vivo production and purification of circular RNA aptamer. *J. Biotechnol.* **139**, 265–272 (2009).
59. Schindelin, J. et al. Fiji: an open-source platform for biological-image analysis. *Nat. Methods* **9**, 676–682 (2012).

nature research

Corresponding author(s): Samie R. Jaffrey

Reporting Summary

Nature Research wishes to improve the reproducibility of the work that we publish. This form provides structure for consistency and transparency in reporting. For further information on Nature Research policies, see Authors & Referees and the Editorial Policy Checklist.

Statistical parameters

When statistical analyses are reported, confirm that the following items are present in the relevant location (e.g. figure legend, table legend, main text, or Methods section).

n/a	Confirmed	
☐	☒	The exact sample size (*n*) for each experimental group/condition, given as a discrete number and unit of measurement
☐	☒	An indication of whether measurements were taken from distinct samples or whether the same sample was measured repeatedly
☒	☐	The statistical test(s) used AND whether they are one- or two-sided *Only common tests should be described solely by name; describe more complex techniques in the Methods section.*
☒	☐	A description of all covariates tested
☒	☐	A description of any assumptions or corrections, such as tests of normality and adjustment for multiple comparisons
☐	☒	A full description of the statistics including central tendency (e.g. means) or other basic estimates (e.g. regression coefficient) AND variation (e.g. standard deviation) or associated estimates of uncertainty (e.g. confidence intervals)
☒	☐	For null hypothesis testing, the test statistic (e.g. *F*, *t*, *r*) with confidence intervals, effect sizes, degrees of freedom and *P* value noted *Give P values as exact values whenever suitable.*
☒	☐	For Bayesian analysis, information on the choice of priors and Markov chain Monte Carlo settings
☒	☐	For hierarchical and complex designs, identification of the appropriate level for tests and full reporting of outcomes
☒	☐	Estimates of effect sizes (e.g. Cohen's *d*, Pearson's *r*), indicating how they were calculated
☐	☒	Clearly defined error bars *State explicitly what error bars represent (e.g. SD, SE, CI)*

Our web collection on statistics for biologists may be useful.

Software and code

Policy information about availability of computer code

Data collection	NIS-Elements 3.22.15, Image Lab 5.0, SnapGene 4.2
Data analysis	NIS-Elements Viewer 4.20, ImageJ 1.51r, and Image Lab 5.2.1 for analyzing images and FlowJo 10.4 for analyzing Flow cytometry data, R 3.4.1 and RStudio 1.0.157 for statistical analysis and data plotting.

For manuscripts utilizing custom algorithms or software that are central to the research but not yet described in published literature, software must be made available to editors/reviewers upon request. We strongly encourage code deposition in a community repository (e.g. GitHub). See the Nature Research guidelines for submitting code & software for further information.

Data

Policy information about availability of data

All manuscripts must include a data availability statement. This statement should provide the following information, where applicable:

- Accession codes, unique identifiers, or web links for publicly available datasets
- A list of figures that have associated raw data
- A description of any restrictions on data availability

The authors declare that all data supporting the findings of this study are available within the paper and its supplementary information files.

Field-specific reporting

Please select the best fit for your research. If you are not sure, read the appropriate sections before making your selection.

☒ Life sciences ☐ Behavioural & social sciences ☐ Ecological, evolutionary & environmental sciences

For a reference copy of the document with all sections, see nature.com/authors/policies/ReportingSummary-flat.pdf

Life sciences study design

All studies must disclose on these points even when the disclosure is negative.

Sample size	Four sample replicates were measured for each luciferase assay condition. For measurements for sensor fluorescence in vitro, one sample was measured
Data exclusions	Prior to experiments, we established that dead cells would be excluded from analysis based on morphological features (e.g. cell detachment and shrinkage).
Replication	Data from the following panels were independently reproduced once (2b,c,d, 3c,d,e, 4b,c, 5c, S1c, S3a,b,c, S4a, S5b, S7a,d), twice (2a, 3b, 5d, S5a, S7c, S9a,b, S10b,c,e), or thrice (3a, S8) with similar results
Randomization	Except dead cells, cells from representative random fields were used for analysis.
Blinding	The investigators were not blinded to group allocation.

Reporting for specific materials, systems and methods

Materials & experimental systems

n/a	Involved in the study
☒	☐ Unique biological materials
☐	☒ Antibodies
☐	☒ Eukaryotic cell lines
☒	☐ Palaeontology
☒	☐ Animals and other organisms
☒	☐ Human research participants

Methods

n/a	Involved in the study
☒	☐ ChIP-seq
☐	☒ Flow cytometry
☒	☐ MRI-based neuroimaging

Antibodies

Antibodies used	Rig-I D14G6 (Cell Signaling Technologies, cat# 3742, lot# 2,), Cleaved PARP (Asp214) (D64E10) (Cell Signaling Technologies, cat# 5625, lot# 13), GAPDH G-9 (Santa Cruz Biotechnologies, sc365062, lot# A2816), all at 1:1000 working dliution.
Validation	Antibodies are validated by the manufacturer as follows. Rig-I D14G6 was validated by LPS stimulation. Cleaved PARP (Asp214) (D64E10) was validated with staurosporine, etoposide, or cycloheximide/TNF-a treatment. GAPDH G-9 was validated by simultaneous direct detection alongside beta-actin detection as well as by cell immunofluorescence and tissue immunoperoxidase staining.

Eukaryotic cell lines

Policy information about cell lines

Cell line source(s)	The following cell lines were obtained directly from the American Type Culture Collection (ATCC): HEK293T (ATCC-CRL-11268), HeLa (ATCC-CCL-2), HepG2 (ATCC-HB-8065), and COS-7 (ATCC-CRL-1651). NFkB reporter HEK293 recombinant cell line was sourced from BPS Bioscience.
Authentication	The cell lines were recently purchased prior to use, but were not additionally authenticated
Mycoplasma contamination	Cells were screened for mycoplasma contamination before passaging using mycoplasma contamination using Hoechst 33258, according to ATCC recommendations.

Commonly misidentified lines (See ICLAC register)	No commonly misidentified cell lines were used.

Flow Cytometry

Plots

Confirm that:

☒ The axis labels state the marker and fluorochrome used (e.g. CD4-FITC).

☒ The axis scales are clearly visible. Include numbers along axes only for bottom left plot of group (a 'group' is an analysis of identical markers).

☒ All plots are contour plots with outliers or pseudocolor plots.

☒ A numerical value for number of cells or percentage (with statistics) is provided.

Methodology

Sample preparation	Adherent cell lines were harvested from culture using trypsin.
Instrument	The Influx Cell Sorter and LSRFortessa instruments from Becton-Dickinson were used for all experiments
Software	BD FACSDIVA software was used for data collection and FlowJo was used for analysis.
Cell population abundance	Populations contained similar levels of green-fluorescent cell fractions (15-20% of total events), which was determined using DIVA software. For analysis experiments without sorting, nearly the entire popoulation (>99.5%) was analyzed.
Gating strategy	Cell were initially gated according to FSC-A and SSC-A according to the observed singlets and doublets, selecting only singlets. Subsequently, the majority population showing relatively lower DAPI signal were selected for gating.

☒ Tick this box to confirm that a figure exemplifying the gating strategy is provided in the Supplementary Information.